On regional modeling of the main geomagnetic field

Giuli Verbanac[1,2]

[1] GeoForschungsZentrum Potsdam, Telegrafenberg, Potsdam, Germany

[2] Department of Geophysics, Faculty of Science, University of Zagreb, Zagreb, Croatia

In this study I applied Spherical Cap Harmonic Analyses, SCHA, with physical regularization (Korte and Holme, 2003) to synthetic series obtained from the Comprehensive model CM4 (Sabaka et al., 2004), at 46 European observatory locations and additionally 11 'virtual observatories' chosen to improve the initial data distribution.

The main purpose was to find an approach for minimising the known drawbacks of SCHA, and to test different effects on the model results, in order to get a tool which allows a better representation of the geomagnetic main field and its secular variation over restricted areas, as Europe is. I also show that an adequate selection of model parametrisation (spherical cap angle, maximal spherical cap harmonics order, number of splines, norms) and a physical regularization allow that model smoothness and misfit are those required by the data themselves. The misfit of the final model was tested using different criteria: the rms values, the time evolution of the coefficients and the behaviour of the original versus modeled time series at each location. Models computed for different epochs satisfy the proposed validation criteria, underlining the reliability to compute stable models over the whole considered time span.

This study opens a way to describe in detail regional geomagnetic main field and its secular variation.

Keywords: Geomagnetic field, secular variation, regional modelling, spherical cap harmonic analyses, comprehensive models.

1. Introduction

The terrestrial magnetic field is a very complex system with contributions from different sources. As observed on the Earth's surface, the field contains components of internal (core and lithospheric fields) and external origins (ionospheric and magnetospheric fields). The geomagnetic field changes on different space and time scales. The core field represents the dominant part of the Earth's magnetic field and its variation over time scales of decades to centuries is referred to as secular variation (henceforth SV). The lithospheric field

includes sources located both in the upper mantle and in the crust, varying from fractions of nT to several thousand nT. The spatial variations in that field are associated with different geological properties of the crust. The ionospheric and magnetospheric fields are respectively related to ionospheric current systems (equatorial and polar electrojets) and magnetospheric currents (in magnetopause in the direction of the Sun; tail currents; ring currents surrounding equatorial region at a distance of several Earth radii). The values of those fields at the Earth's surface are of few tens of nT, but can reach few hundred, even thousand nT during magnetic storms. The variations with periods from seconds to one year are generally external in origin.

Different models try to fit and explain the observed geomagnetic field and its time variations on global as well as on regional scales. Among global models, frequently used are International Geomagnetic Reference Field (Macmillan et al., 2003) and Comprehensive Model CM4 (Sabaka et al., 2004). The purpose of modern regional modelling is to describe the geomagnetic field over a portion of the Earth's surface, providing a better spatial resolution of the local field for areas of high data density. There are large demands for detailed information of the elements of the main field and its SV, like in land surveys, mineral explorations, navigation and in many scientific studies (study of the core dynamic, lithospheric field). In the following I focus on the regional modelling techniques, only.

The first 'models' over regions of the Earth's surface were hand drawn charts, as the one produced by Halley in 1700 (Clark, 2000). These representations are not precise, however they have been used during the last three centuries. Recently, fitting regional surface polynomials in latitude and longitude to various components has been widely applied. These polynomials are not function of radial distance, so there is no possibility for upward or downward continuation.

During the last few decades new methods as Component Rectangular harmonic analyses using rectangular instead of spherical coordinates (Alldredge, 1981) and Spherical harmonic analyses SCHA (Haines, 1985) have been introduced. Recently, two approaches for improving spherical harmonic modeling have been proposed: a physical method of regularization (Korte and Holme, 2003) and revised SCHA, named R-SCHA (Thébault et al., 2006; Thébault et al., 2004). The basic concept of SCHA is expansion, in terms of spherical coordinates, of the magnetic potential in two sets of basis functions that satisfy Laplace's equation within the chosen cap area.

Korte and Holme (2003) adopted the original SCHA by replacing statistical regularization with the more meaningful physical regularization. Instead of setting the coefficients that are considered as statistically insignificant to zero, the approach of physical regularization suggests minimisation of the certain feature of the field (i.e. field energy). Additionally, they used cubic splines as basis functions for simultaneously modeling in time and space. This study follows their approach and is described in detail in the following section. The

R-SCHA formalism enables properly modeling the radial variation of the field by solving the boundary value problem in a region bounded by the 1) Earth's surface, 2) an upper surface corresponding to available satellite data and 3) a conical surface to enclose the region under study. The reconstruction of the real field showed that the residuals are maximal at the Earth's surface, so this method is not yet appropriate for modeling only ground data. However, it improves dramatically the representation of the crustal field, when data available from different platforms (ground, aeromagnetic, satellites) are used.

Let me note, that there are, also new attempts to develop regional models based on wavelet analyses (Holschneider et al., 2003; Chambodut et al., 2005). These methods are still in a developing phase and have only been applied to synthetic, noise-free data so far. Moreover, time dependent models have not yet been tested.

All regional modeling techniques inherently have problems of edge effects near the regional boundaries and imperfect spatial data distribution can lead to further artificial structures. The currently available method to obtain continuous regional descriptions of main field and secular variation is regularised SCHA. This method has been widely used (Haines and Newitt, 1986; Garcia et al., 1991; Torta et al., 1992; De Santis et al., 1997; Kotzé, 2001). Although some satisfying results were obtained, a few problems were encountered. For example, the results get worse as the cap becomes smaller because for a small cap high degree expansion is necessary in order to include large wavelengths. This may be a problem if there is no enough data available. It was also noticed that SCHA fails in correctly describing the radial dependence. The present study aims at understanding the influence of mathematical shortcomings and data distribution and demonstrating what accuracy can be expected from this modeling method.

I focused on the European region and the time span 1960.5–2001.5, because that is the region and time of highest spatial coverage with high-quality ground data. At most European geomagnetic observatories near-continuous time-series exist for that interval. Since even these time-series contain unreported errors (Verbanac et al., 2007), I considered as the best strategy to first verify the validity of the SCHA method when applied to synthetic data of the same spatio-temporal distribution. Synthetic data can be considered as error-free, leading to an easier interpretation of the modelling results. Moreover, it enables to distinguish artificial effects caused by data errors from those caused by insufficient mathematical description of the real phenomena. From the CM4 model (Sabaka et al., 2004), synthetic data were obtained at locations of 46 European observatories and additionally at 11 locations between the observatories and the cap boundary (henceforth žvirtual observatories').

The aim of this study was to model the main field using only ground data with SCHA. A few parameters in the modelling process were tested (spherical cap harmonic angle, maximal degree of the spherical cap harmonic expansion, temporal splines, norms, regularization factors) to find the appropriate ones.

The choice of parameters allowed me to model the main field over a restricted region as Europe.

This paper is organised as follows. In the next section I give a theoretical overview of the used modelling method (SCHA), regularization technique and temporal modelling with splines. Then, the descriptions of synthetic data and the attempt of their reconstruction are presented. Further, I show and explain the obtained results and finally discuss them.

2. Modeling Method

2.1. Spherical cap harmonic analyses

In a source-free region, the magnetic field **B** can be represented as the negative gradient of the scalar potential Φ, **B** $= -\nabla\Phi$, where Φ has to satisfy the Laplace's equation: $\nabla^2\Phi = 0$. The solution is obtained by the method of spherical harmonic analyses and is given in terms of Legendre polynomials in co-latitude and trigonometric functions in longitude.

When observations are available only over the small portion of the Earth or analyses is required only over the restricted region, the same Legendre polynomials and trigonometric functions are no longer the appropriate basis functions. The problem arises because the least square matrix of normal equations is often ill conditioned and cannot be solved with a sufficient degree of accuracy.

Haines (1985) introduced spherical cap harmonics for use over the polar cap of half-angle θ_0. He proposed the method termed, Spherical cap harmonic analyses, to analytically solve the boundary value problem in order to fit a differentiable potential over a spherical cap. The boundary conditions have to enable potential expansion in a uniformly convergent series of basis functions.

The general solution of the Laplace's equation in the case of SCHA is:

$$\Phi(r,\theta,\phi) = R_E \sum_{k=0}^{k_{max}} \sum_{m=0}^{k} \left(\frac{R_E}{r}\right)^{n_k+1} [g_k^m \cos(m\phi) + h_k^m \sin(m\phi)] P_{n_k}^m (\cos\theta). \quad (1)$$

The potential is a function of radius r, colatitude θ and longitude ϕ. R_E is the mean radius of the Earth and $\{g_k^m, h_k^m\}$ are the SCHA coefficients, the $\{P_{nk}^m\}$ are the associated Legendre functions with non-integer degrees n_k and integer orders m. The value of n have to be non-integer in order to keep, as far as possible, the orthogonality of the harmonics over the cap. This implies that $\{P_{n_k}^m(\cos\theta)\}$ are no longer polynomials with a finite linear combination of powers. The order of Legendre functions remains integer enabling the continuity of the potential in longitude.

For the whole sphere the potential must satisfy conditions in longitude, meaning that both the potential and its derivative must have same values

when $\phi = 0$ and when $\phi = 2\pi$. Regarding to co-latitude, the potential and its derivative are forced to be zero at the poles ($\theta = 0$ or π) depending on the order m, forcing the degree n to be an integer:

$$\frac{\partial \Phi_n^m}{\partial \theta} = 0 \ \ \text{for } m = 0, \tag{2}$$

$$\Phi_n^m = 0 \ \ \text{for } m \neq 0.$$

When the analyses is restricted to a spherical cap, $\theta \neq \pi$, the same boundary conditions are valid in longitude, but when $\theta = \theta_0$:

$$\frac{\partial \Phi(r, \theta_0, \phi)}{\partial \theta} = g(r, \phi), \tag{3}$$

$$\Phi(r, \theta_0, \phi) = f(r, \phi). \tag{4}$$

Equation 3 is valid when the degree n_k is such that:

$$P_{n_k}^m = 0 \ \ \text{at the cap boundary.} \tag{5}$$

Equation 4 is valid when the degree n_k is such that:

$$\frac{\partial P_{n_k}^m}{\partial \theta} = 0 \ \ \text{at the cap boundary.} \tag{6}$$

Each value of m gives two series of values of n. When $(k - m)$ is even the roots of Equation 6 are obtained and $(k - m)$ is odd gives the roots of Equation 5. However, the orthogonality is no longer complete: the two sets of basis functions $((k - m) = \text{even}, (k - m) = \text{odd})$ are mutually orthogonal in each set, but those from one set are not always orthogonal with those in the other. This is reflected in a scalar products of the functions being different from zero:

$$\int_0^{\theta_0} P_{n_j}^m(\cos\theta) P_{n_k}^m(\cos\theta) \sin\theta \, d\theta = -\frac{\sin\theta_0}{[n_k - n_j][n_k + n_j + 1]} P_{n_j}^m(\cos\theta_0) \frac{dP_{n_k}^m(\cos\theta_0)}{d\theta} \tag{7}$$

for $(j - m)$ even and $(k - m)$ odd,

$$\int_0^{\theta_0} [P_{n_k}^m(\cos\theta)]^2 \sin\theta \, d\theta = -\frac{\sin\theta_0}{2n_k + 1} P_{n_k}^m(\cos\theta) \frac{\partial}{\partial n_k} \frac{dP_{n_k}^m(\cos\theta_0)}{d\theta} \tag{8}$$

for $(k - m)$ even and

$$\int_0^{\theta_0} [P_{n_k}^m(\cos\theta)]^2 \sin\theta \, d\theta = \frac{\sin\theta_0}{2n_k+1} \frac{dP_{n_k}^m(\cos\theta_0)}{d\theta} \frac{\partial}{\partial n_k} P_{n_k}^m(\cos\theta) \qquad (9)$$

for $(k - m)$ odd. Equations 8 and 9 follow from the Equation 7, using L'Hô-pital's rule in the limit that n_k tends to n_j.

The accuracy by which the Legendre functions are computed greatly influ-ences the SCHA results. The original subroutine for computing these func-tions (Haines, 1985) encountered often lack of convergence of the series lead-ing to the incorrect values of $\{P_{n_k}^m(\cos\theta)\}$. Especially, the problem arises for large value of degree n_k or high values of latitude. Thébault et al. (2002) showed that more appropriate way to compute the values of associated Le-gendre functions is the algorithm proposed by Olwer and Smith (1983), which uses extended-range arithmetic subroutines. Using a double, instead of a sin-gle precision (as in the original code given by Haines (1985)) increases the pre-cision of computed roots, n_k.

2.2. The least-squares estimators and regularization of the inverse problem

A mathematical model can be derived by linear inversion method. The lin-ear system of equations is given:

$$y = \mathbf{Am} + \text{e}, \qquad (10)$$

where y is the data vector, $\mathbf{A}$ is the operator mapping the data vector to the model vector $\mathbf{m}$ and e is the error vector. The classical approach to solve such problem is to minimize the differences between the observed and modeled data. The normal equations are:

$$\mathbf{A}^T\mathbf{Am} = \mathbf{A}^T y, \qquad (11)$$

which give the maximum likelihood solution when errors have a non-uniform variance:

$$\hat{\text{m}} = (\mathbf{A}^T\mathbf{C}_e^{-1}\mathbf{A})^{-1}\mathbf{A}^T\mathbf{C}_e^{-1}y. \qquad (12)$$

$\mathbf{C}_e$ is the data error covariance matrix.

To stabilise the solution and in order to ensure that model structures are those required by data, so that data are not over-fit with their errors, the method has to be regularized. There are two kinds of regularization: statistical and physical. In the statistical regularization coefficients that are considered as statistically insignificant are set to zero. The physical regularization em-ploys the minimisation of a certain features of the field over the cap surface.

When using the regularization technique, the following function has to be minimized:

$$(y - \mathbf{Am})^T \mathbf{C}_e^{-1}(y - \mathbf{Am}) + \lambda \mathbf{m}^T \Lambda \mathbf{m}. \tag{13}$$

The regularization is given by the $\mathbf{m}^T \Lambda \mathbf{m}$ term, which is a quadratic norm of smoothness of the field over the spherical cap. Λ is a damping matrix. λ is a Lagrange multiplier. The maximum likelihood solution is similar to (12):

$$\hat{\mathrm{m}} = (\mathbf{A}^T \mathbf{C}_e^{-1}\mathbf{A} + \lambda\Lambda)^{-1}\mathbf{A}^T \mathbf{C}_e^{-1}y. \tag{14}$$

The damping matrix is determined by the norm. In SCHA the damping matrix is not diagonal, because the basis functions are not completely orthogonal. However, the integral of products of functions with $m \neq m'$ are zero, so most of the non-diagonal elements in the damping matrix are zero.

One regularization possibility is to minimize only the mean square radial component of $\mathbf{B}$, B_r^2, square norm of the total field $\mathbf{B}$, $\mathbf{B}^2$, or the combine norm of the squared radial derivative of the radial component and squared field, $(d\mathbf{B}/dr)^2 + \mathbf{B}^2$. The minimization of the mean square radial component of $\mathbf{B}$ is given by:

$$\left\langle B_r^2 \right\rangle = \sum_{n_k} \sum_{n_j} \sum_{m} (g_{n_k}^m g_{n_j}^m + h_{n_k}^m h_{n_j}^m)(n_k + 1)(n_j + 1)\left(\frac{R_E}{r}\right)^{(n_k + n_j + 4)} a$$

$$\cdot \int_{\theta=0}^{\theta_0} P_{n_k}^m(\cos\theta)P_{n_j}^m(\cos\theta)\sin\theta d\theta, \tag{15}$$

where the θ – integral is given by Equations 7–9. The symbol $\langle \ldots \rangle$ refers to the mean over the cap and the factor a is the result of the ϕ – integral, 2π for $m = 0$, π for $m \neq 0$, normalised for the area of the cap, $2\pi\,(1 - \cos\theta)$:

$$a = \begin{cases} 1/(1 - \cos\theta_0) & : \quad m = 0 \\ 1/(2(1 - \cos\theta_0)) & : \quad m \neq 0 \end{cases} \tag{16}$$

The square norm of the main field $\mathbf{B}$ is given by:

$$\langle B \cdot B \rangle = \sum_{n_k} \sum_{n_j} \sum_{m} (g_{n_k}^m g_{n_j}^m + h_{n_k}^m h_{n_j}^m)\left(\frac{R_E}{r}\right)^{(n_k + n_j + 4)} \left[\sin\theta_0 P_{n_j}^m(\cos\theta_0)\frac{dP_{n_k}^m(\cos\theta_0)}{d\theta} \right.$$

$$\left. + (n_k + n_j + 1)(n_k + n_j + 2)\frac{a}{2}\int_{\theta=0}^{\theta_0} P_{n_k}^m(\cos\theta)P_{n_j}^m(\cos\theta)\sin\theta d\theta \right] \tag{17}$$

The first term in the square bracket vanishes for $k = j$, $(k - m)$ odd, or $(j - m)$ even, as either $P_n^m(\cos\theta_0)$ or $dP_n^m(\cos\theta_0)/d\theta$ is zero due to the boundary conditions. Considering this norm, the elements of the damping matrix Λ are:

$$f_{kj} = \left(1 - \frac{(n_k + n_j + 2)}{(n_j - n_k)}\right)\left(\frac{R_E}{r}\right)^{(n_k + n_j + 4)} \frac{a}{2} \sin\theta_0 P_{n_k}^m(\cos\theta_0)\frac{dP_{n_j}^m \cos\theta_0}{d\theta} \quad (18)$$

for the non-diagonal elements with $m = m'$, $(k - m)$ even and $(j - m)$ odd,

$$f_{kk} = -(n_k + 1)\left(\frac{R_E}{r}\right)^{(2n_k + 4)} a \sin\theta_0 P_{n_k}^m(\cos\theta_0)\frac{\partial}{\partial n_k}\frac{dP_{n_j}^m \cos\theta_0}{d\theta} \quad (19)$$

for the diagonal elements with $(k - m)$ even and

$$f_{kk} = (n_k + 1)\left(\frac{R_E}{r}\right)^{(2n_k + 4)} a \sin\theta_0 \frac{dP_{n_j}^m(\cos\theta_0)}{d\theta}\frac{\partial}{\partial n_k}P_{n_k}^m(\cos\theta_0) \quad (20)$$

for the diagonal elements with $(k - m)$ odd.

Expressions for $(dB_r/dr)^2$ and $(d\mathbf{B}/dr)^2$ norms contain only an additional factor:

$$(n_k + 2)(n_j + 2)\left(\frac{R_E}{r}\right)^2, \quad (21)$$

in respect to B_r^2 and $\mathbf{B}^2$ norms.

All these equations are also valid for secular variation $\mathbf{B}$ when substituting the time derivative of the coefficients $\{\dot{g}_k^m, \dot{h}_k^m\}$.

2.3. Temporal modeling with cubic splines

A practical problem that very often arises when analysing geomagnetic data is how to fit a smooth function to a time series of observations. One approach can be to use smoothing splines for estimating the unknown function. The natural spline functions $S(\xi)$ is a linear combination of B-spline functions:

$$S(\xi) = \sum_{j=-1}^{n+1} a_j B_{j,k}(\xi), \quad (22)$$

a_j are the spline coefficients and $B_{j,k}(\xi)$ are the piecewise polynomial functions of order k. A B-spline function is defined on the whole real line, but extended by zero outside interval $[t_1, t_j]$. This interval is subdivided into $n + 2$

spans by division points, knots, that are $t_0 \le t_1 \le \ldots \le t_j$. The i-th B-spline of degree k is defined recursively through the Cox-DeBoor formula:

$$B_{i,1} = \begin{cases} 1 & t_i \le \xi < t_{i+1} \\ 0 & \text{otherwise} \end{cases}, \tag{23}$$

and for $k \ge 1$

$$B_{ik}(\xi) = \frac{\xi - t_i}{t_{i+k-1} - t_i} B_{i,k-1}(\xi) + \frac{t_{i+k} - \xi}{t_{i+k} - t_{i+1}} B_{i+1,k-1}(\xi) . \tag{24}$$

The B-splines are for $k = 2$ piecewise linear, for $k = 3$ piecewise quadratic, for $k = 4$ piecewise cubic, etc. For simple smoothing splines, the knots t_j are chosen to be the data points. Cubic B-splines with equidistant knots are given as:

$$B_{i,4}(\xi) = \begin{cases} 1/6 z^3 & t_{i-2} < \xi < t_{i-1}, \\ 1/6 \left[1 + 3(1 + z(1-z))z \right] & t_{i-1} \le \xi < t_i, \\ 1/6 \left[1 + 3(1 + z(1-z))(1-z) \right] & t_i \le \xi < t_{i+1}, \\ 1/6 (1-z)^3 & t_{i+1} \le \xi < t_{i+2}, \\ 0 & \text{otherwise}, \end{cases} \tag{25}$$

where the distance between the knots is $d = t_{i+1} - t_i$ and z is given as $z = (\xi - t_{i+2})/d$. A more detailed discussion of splines and B-spline basis is given by (de Boor, 1978).

In this study each of the SCHA coefficients is expanded in time as a linear combination of cubic B-splines $B_j(t)$:

$$g_{n_k}^m(t) = \sum_{j=1}^{L} \alpha_{jkm} B_{j,4}(t) . \tag{26}$$

The α_{jkm} are temporal coefficients determined by minimizing following functional:

$$(y - \mathbf{Am})^T \mathbf{C}_e^{-1} (y - \mathbf{Am}) + \int \left[\lambda \int \mathbf{B}^2 d\Omega + \tau \int \left(\frac{\partial^2 \mathbf{B}}{\partial t^2} \right)^2 d\Omega \right] dt \tag{27}$$

The three terms minimize the data misfit, spatial roughness (λ) and temporal roughness (τ), respectively. λ and τ are Lagrange multipliers controlling the trade off of the misfit and roughness criteria.

3. Data And Modeling Parametrisation

3.1. Data

In this study only synthetic, noise-free data were considered. To estimate the main field components at a given location and given epoch, the CM4 code was used. This model takes into account various contributions to the actual magnetic field: core, crust, primary magnetospheric, secondary (induced) magnetospheric, primary ionospheric, secondary (induced) ionospheric, toroidal magnetic field due to in-situ radial currents at satellite altitude. In order to consider only the core field, I used spherical harmonic expansion up to degree/order 13. The CM4 model (Sabaka et al., 2004) is a continuous model covering the time-span 1960–2002 and, among other global models in use, has a very good data-to-noise ratio. Due to these advantages, this study was based on the dataset produced with this model for the period of its validity.

The X (northward), Y (eastward) and Z (vertically downward) components of the main field given by CM4 were produced at 57 locations, 46 of them being real observatory sites and the remaining 11 locations of 'virtual observatories' (see Figure 1).
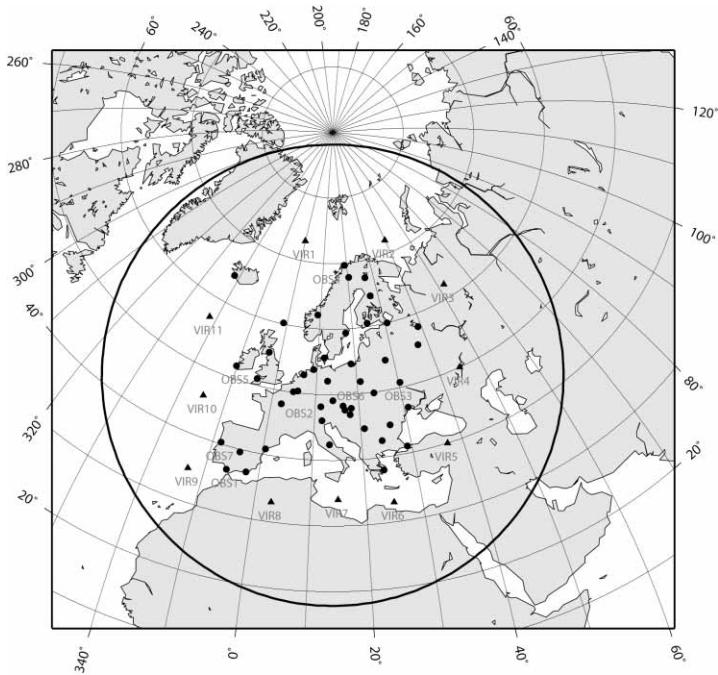
Figure 1. Locations of the geomagnetic observatories (full circles) and virtual observatories (triangles) for which synthetic datasets are computed from CM4 model. The large circle shows the border of the spherical cap of $\theta_0 = 35°$ used for the SCHA-modelling.
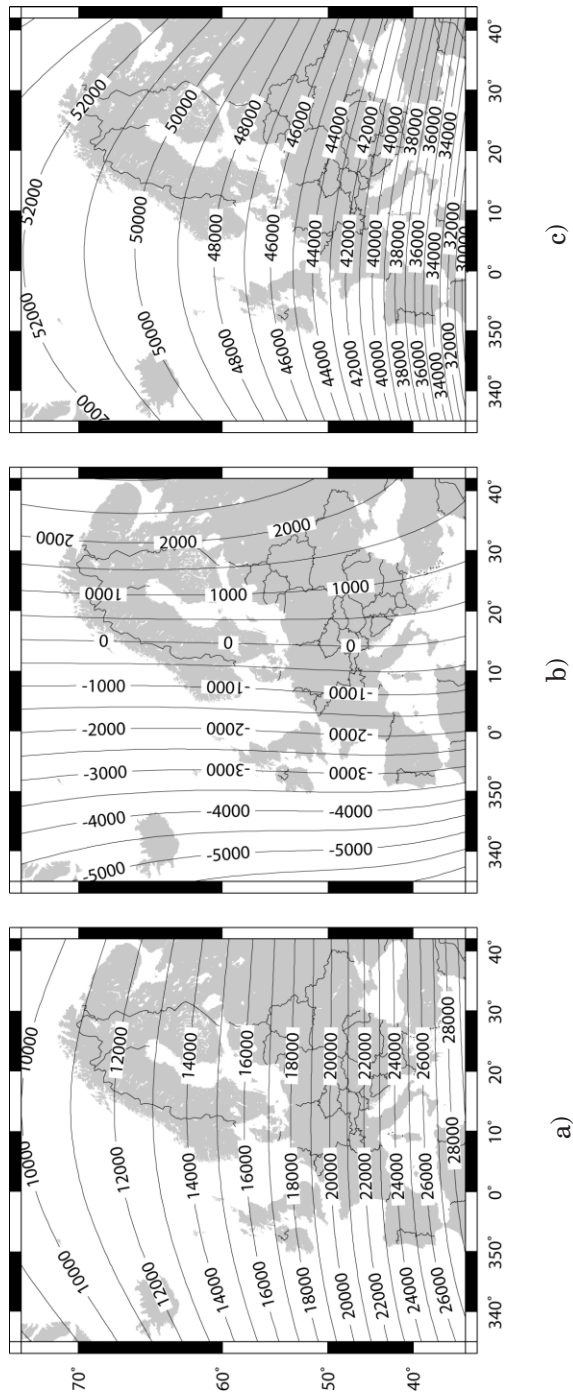
Figure 2. Maps at epoch 1980.5 for the main field (EU_1X1_CM4) of the X (a), Y (b) and Z (c) components, in nT, computed from the CM4 model on the regular grid of 1° × 1°.

In order to verify the consistency of the proposed modelling method, I estimated from the CM4 model synthetic data for the three components of the main geomagnetic field on a regular grid of $1° \times 1°$ in the considered region (henceforth EU_1X1_CM4). The maps are shown in Figure 2 and they represent the reference maps for the following comparison.

3.2. Modelling parametrisation

In the following I define the parameters for this specific SCHA: spherical cap angle, maximal spherical cap harmonics order, number of splines, norms, damping factors.

Spherical cap angle. The region to be studied has to be defined by a spherical cap well covering that area, with margins large enough around it in order to prevent, as far as possible, the influence of the cap boundary. I chose the spherical cap half angle of 35° (Figure 1), which satisfies the above criteria. The cap centre is located at 53°N latitude and 14°E longitude.

Maximal spherical cap harmonics order. In order to chose the maximum spherical cap harmonics order, k_{max}, two criteria were considered. Firstly, the model has to be controlled by the used dataset and not by the spherical expansion truncation level. Secondly, this model has to describe the long wavelengths of the core field (dipol) over the portion of the Earth. In this case, a larger degree for the expansion is required, sometimes even larger then allowed by the number of available data. For this reason, the convergence of the expansion becomes slower with increasing k_{max}.

I started my computation with the highest k_{max} which allows the system to be solved. For $k_{max} = 9$, numerical problems were encountered, probably as a consequence of incomplete orthogonality of the basis functions, but numerical damping for stability was not applied and all models were obtained with $k_{max} = 8$.

One of the advantages of the SCHA is that the degree n_k, represents the number of minimum representable wavelengths, like in SHA:

$$\lambda_{\min} = 2R_E\pi/n_k, \tag{28}$$

where R_E is the Earth's mean radius (6371.2 km). The approximate relation between k_{max}, n_k, and θ_0 (Haines, 1988) is given by:

$$n_k = \left(\frac{90°}{\theta_0}\right)(k_{\max} + 0.5) - 0.5 \tag{29}$$

allowing λ_{min} estimation. In our case $\lambda_{min} = 1880$ km ($n_k = 21.3$) compared to some 3000 km covered by the spherical harmonic degree 13.

Temporal splines. For temporal modelling with splines, I chose 20 knots points. In total 1620 coefficients were calculated, 81 per each knot point. The SHA, describing the same wavelength $\lambda_{min} = 1880$ km would require 483 coef-

Table 1. The rms values for the computed models at epoch 1980.5.

Model	Nb of locations	Nb. of used data[1]	Model rms (nT)	Total rms[2] (nT)
CM4_OBS_NOR	46	5796	7	2400
CM4_OBS_R	46	5796	25	813
CM4_OBS_VIR_NOR	57	7182	9	307
CM4_OBS_VIR_R	57	7182	11	215

[1] Total number of X, Y and Z data for the used locations over 42 years.
[2] The rms for 7182 residuals, computed on the regular $1° \times 1°$ grid.

ficients (indeed an expansion up to degree/order 21) per knot point, some six times more than with SCHA (81 coefficients).

Damping factors. Special attention was paid to find the best damping factors, λ (spatial) and τ (temporal). Because the misfit between the data and model prediction is not very sensitive on temporal damping, I first investigated a wide range of spatial and temporal damping factors, searching for which temporal damping the misfit starts to change. Assuming error-free data, I expected to be able to fit data even without damping, so I chose that τ prior to a found change in misfit. Then, keeping τ constant I examined the misfits for a wide range of λ to ensure that the plot of the norm value against a misfit, the so-called trade-of curve, is well defined. Finally, for the λ chosen from the knee of a trade-off curve, I investigated the trade-off curve of the temporal norm against the misfit for wide ranges of τ in order to verify that the τ chosen before is the appropriate one. Again, I noticed that the misfit change very little with τ.

Norms. The combination of two norms, $\mathbf{B}^2$ and $(d\mathbf{B}/dr)^2$, was used for spatial regularization, following the results by Korte and Holme (2003). The temporal norm was the second derivative of the chosen spatial norm.

Final validation. Once the appropriate damping factors were found, the SCHA model was computed and the residuals (differences between data and model predictions) were calculated on the $1° \times 1°$ grid. As already mentioned, because of method limitations, it is important to verify the quality of the obtained model by considering different criteria. Therefore, I investigated the behaviour of the SCHA coefficients, by plotting the values of the first four coefficients $\left\{ g_0^0, g_1^0, g_1^1, h_1^1 \right\}$ versus time.

Finally, when calculated residuals and time evolution of the coefficients were accepted, the developed model was my 'preferred model'. This was further confirmed by comparing the time series of the original with modeled data at each location, to be fully confident in the reconstruction of the regional field.

4. Results: Modeling CM4 main field by SCHA

4.1. At observatory locations

Following the above explained steps, I fitted the model to the synthetic data for observatory locations.

Data were first modeled without any damping, then with spatial and temporal dampings: $\lambda = 10^{-3}$ and $\tau = 10°$, based on the knee of the trade-off curves (see Fig. 3 for spatial trade-off curve). The model obtained without regularization is named CM4_OBS_NOR and the one with regularization CM4_OBS_R. Figure 4 shows the reconstructed field components for both examined cases and for the epoch 1980.5 (all maps presented in this study are for this epoch). Note also that the region of interest is defined by the area covered by the real observatory locations. Comparison of obtained maps with EU_1X1_CM4 ones (Figure 2) shows that even the model without regularization, CM4_OBS_ NOR, is able to well reconstruct the EU_1X1_CM4 values (Figure 4a). However, some spatial damping is needed in order to get the field smoother (Figure 4b). The rms of both models and number of data used for modelling are listed in Table 1. Model CM4_OBS_NOR has smaller rms compared to CM4_
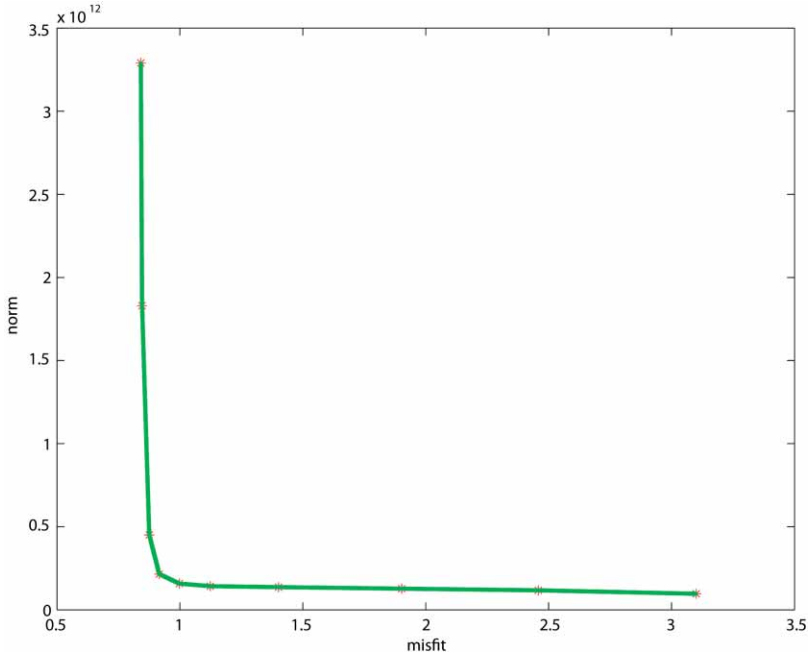
Figure 3. Trade-off curve of the spatial norm vs. misfit. Synthetic data provided by CM4 model at observatory locations were considered.
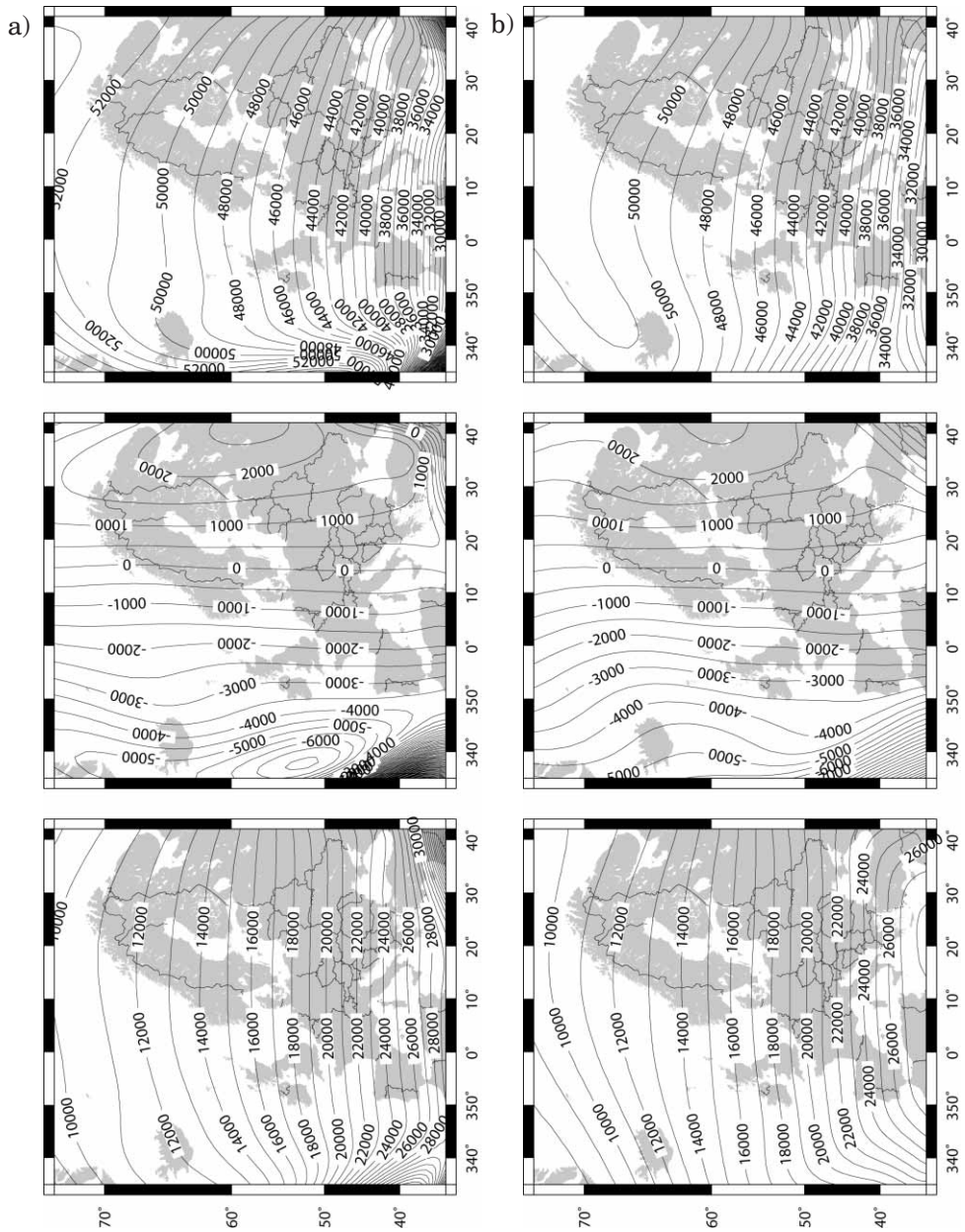
Figure 4. Maps at epoch 1980.5 for the *X* (left), *Y* (centre) and *Z* (right) field components obtained from a SCHA of synthetic data provided by CM4 model at 46 observatory locations shown in Fig. 1: (a) without regularization (model CM4_OBS_NOR) and (b) with regularization, $\lambda = 10^{-3}$ and $\tau = 10^{0}$ (model CM4_OBS_R). Units nT. Mercator map projection.

OBS_R model, as expected, because the regularization increases the smoothness of the model, but at the cost of the fit to the data.

I further calculated the predicted values from both models on the regular $1° \times 1°$ grid and subtracted them from EU_1X1_CM4 values. Corresponding residual maps are presented in Fig. 5. In the very central part of the studied region, the residuals are no higher then about 20 nT in X and Y components, and no larger then 40 nT in Z. The artificial effects that appear outside the region of interest can be noticed on both maps. Near the periphery of the considered grid, their values increase rapidly, showing that extrapolations outside the region of data coverage are not feasible with this method. The computed rms, named total rms, for those residuals are also given in Table 1. These rms values refer to the residuals computed on the regular grid, not only at the observatory locations. Note that here the total rms is lower for CM4_OBS_R model, showing that better results are obtained when regularization is applied.

4.2. At observatory and virtual locations

To improve the spatial distribution and minimize its influence in modelling, in addition to the synthetic data at observatory locations I added eleven virtual observatories located between the cap boundary and observatory sites (see Figure 1). As already explained, these points have not to be situated close to the cap boundary, and not too close to the real observatories, because we want to improve the data distribution without significant influence on the model prediction at the observatory sites.

The new dataset amounts to 7182 data and, as previously, is modeled without any damping (henceforth CM4_OBS_VIR_NOR model), then with damping factors: $\lambda = 10^{-3}$ and $\tau = 10^0$ (henceforth CM4_OBS_VIR_R model) chosen from the knee of the trade-off curves (see Figure 6 for spatial trade-off curve). The resulting maps for 1980.5 are presented in Fig. 7. Comparison of Fig. 4a with Fig. 7a shows that in the later case, the maps are smoother at the edges, even without damping. After regularization with appropriate parameters, the maps are improved as shown in Fig. 7b. Residuals between EU_1X1_CM4 data and both, CM4_OBS_VIR_NOR and CM4_OBS_VIR_R predictions are shown in Figure 8. Models and total rms are listed in Table 1. Again, it is obvious that with the regularization, the field is closely reproduced. To investigate this in more detail, it is instructive to note the CM4_OBS_VIR_R model residuals separately for X, Y and Z component, which are 9 nT, 6 nT and 14 nT, respectively. In the region covered by the grid, the X, Y and Z components are in the ranges $[10000 - 27000 \text{ nT}]$, $[-5000 - 2800 \text{ nT}]$ and $[26000 - 54000 \text{ nT}]$, respectively. For each X, Y and Z component, the residuals count for about 5%, 16% and 3% of the corresponding component mean value. In general, the model tries to fit equally well all components, and the differences of a few nT in individual rms are related to the absolute field component values. It has to be underlined that the highest differences observed nearby boundaries of the
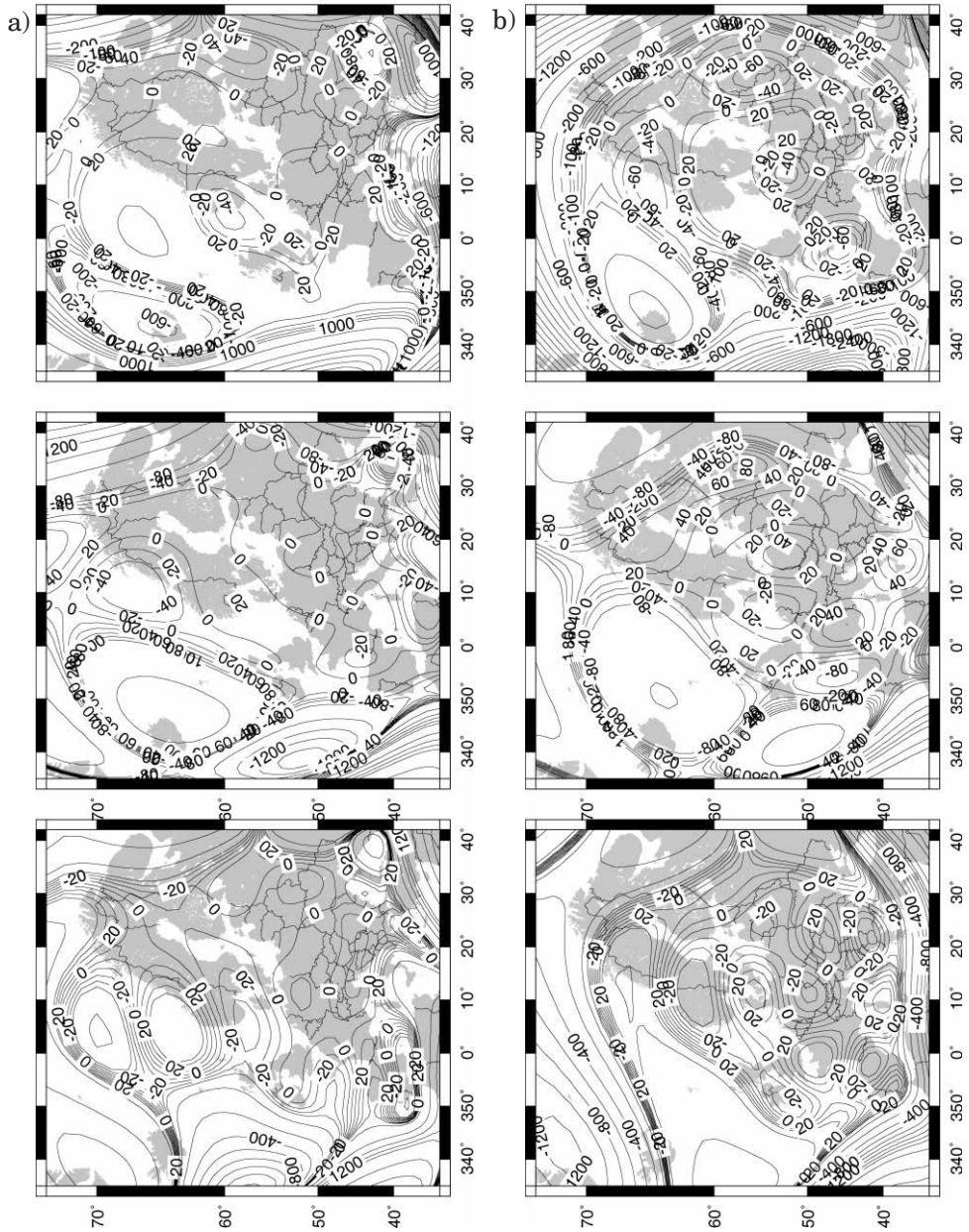
Figure 5. Maps for the X (left), Y (centre) and Z (right) residuals between EU_1X1_CM4 values and (a) CM4_OBS_NOR and (b) CM4_OBS_R model values. Units nT. Mercator map projection.

overall considered region have an influence on the total rms, increasing its value. In the central part of the studied region, namely central Europe, the residuals are no higher then about 10 nT. Nevertheless, satisfying residuals were obtained in the remaining areas of interest, where they do not exceed 20 nT. Note, that the residual map for Z component is dramatically improved with the additional virtual observatories.

Figure 9 reveals smooth changes for the first four SCHA coefficients, $\left\{g_0^0, g_1^0, g_1^1, h_1^1\right\}$, over 42 years. Both $\left\{g_1^0\right\}$ and $\left\{h_1^1\right\}$ show an continuous decreasing trend and $\left\{g_0^0\right\}$ an increasing one. Interestingly, $\left\{g_1^1\right\}$ increases up to the epoch 1980.5, then decreases slightly and remains almost constant until the end of the studied interval. A smooth change of the coefficients, determined by the temporal damping, was expected.

All above mentioned arguments, suggest CM4_OBS_VIR_R as the preferred model. To finally validate CM4_OBS_VIR_R, I investigated how well it fits the synthetic data at individual locations. Very good fit is found at all observatory sites. As example, X, Y and Z components time series at OBS1, OBS2, OBS3, OBS4 and OBS5 (see Figure 1) are presented in Fig. 10. Except OBS2, all these locations are situated at the most outside region covered by observatories, where possibly the largest discrepancies between data and model
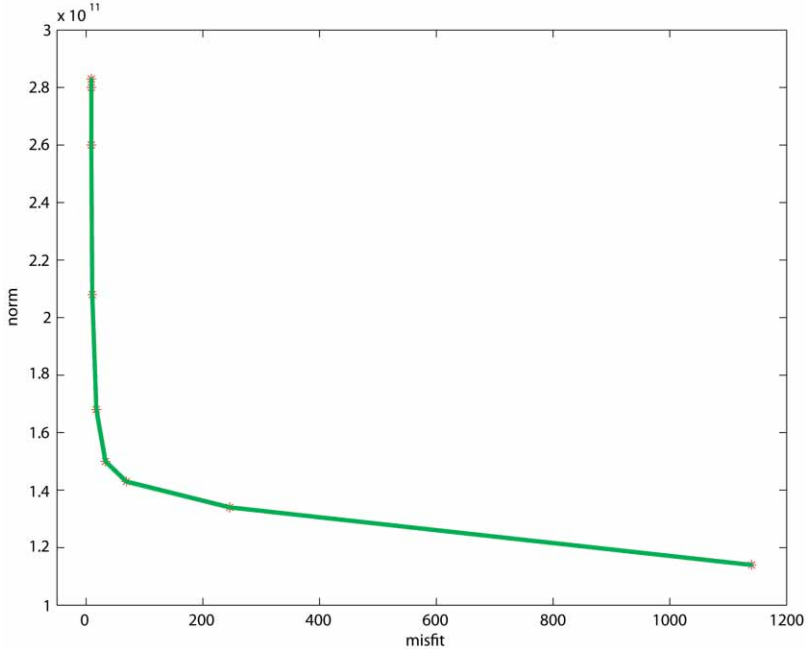

Figure 6. Trade-off curve of the spatial norm vs. misfit. Synthetic data provided by CM4 model at 46 observatory locations and at additional 11 virtual observatory locations were considered (see Fig. 1).
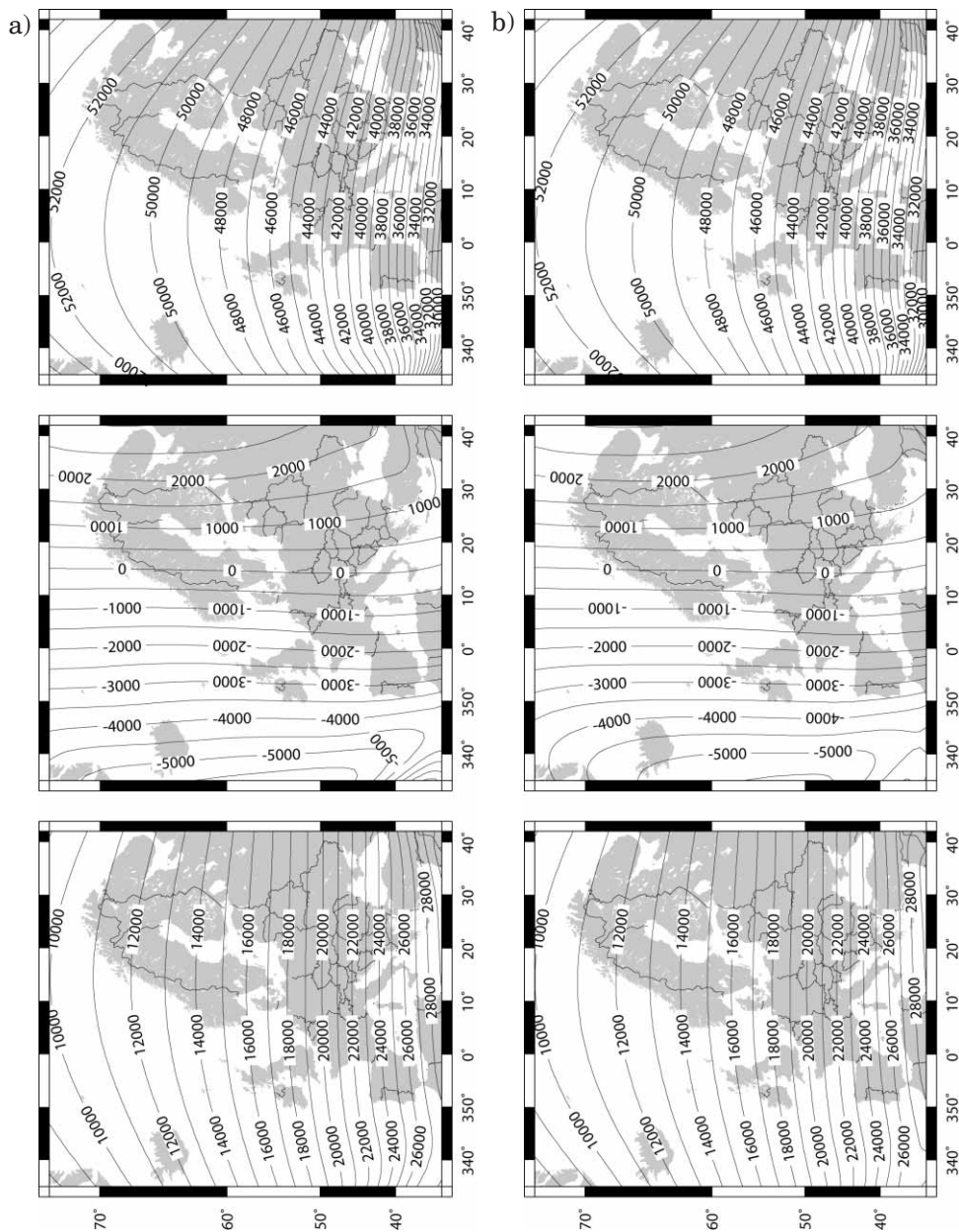
a)

b)

Figure 7. Maps at epoch 1980.5 for the X (left), Y (centre) and Z (right) field components obtained from a SCHA of synthetic data provided by CM4 model at 46 observatory locations complemented with eleven virtual observatories shown in Fig. 1: (a) without regularization (model CM4_OBS_VIR_NOR) and (b) regularization with $\lambda = 10^{-5}$ and $\tau = 10^{0}$ (model CM4_OBS_ VIR_R). Units nT. Mercator map projection.
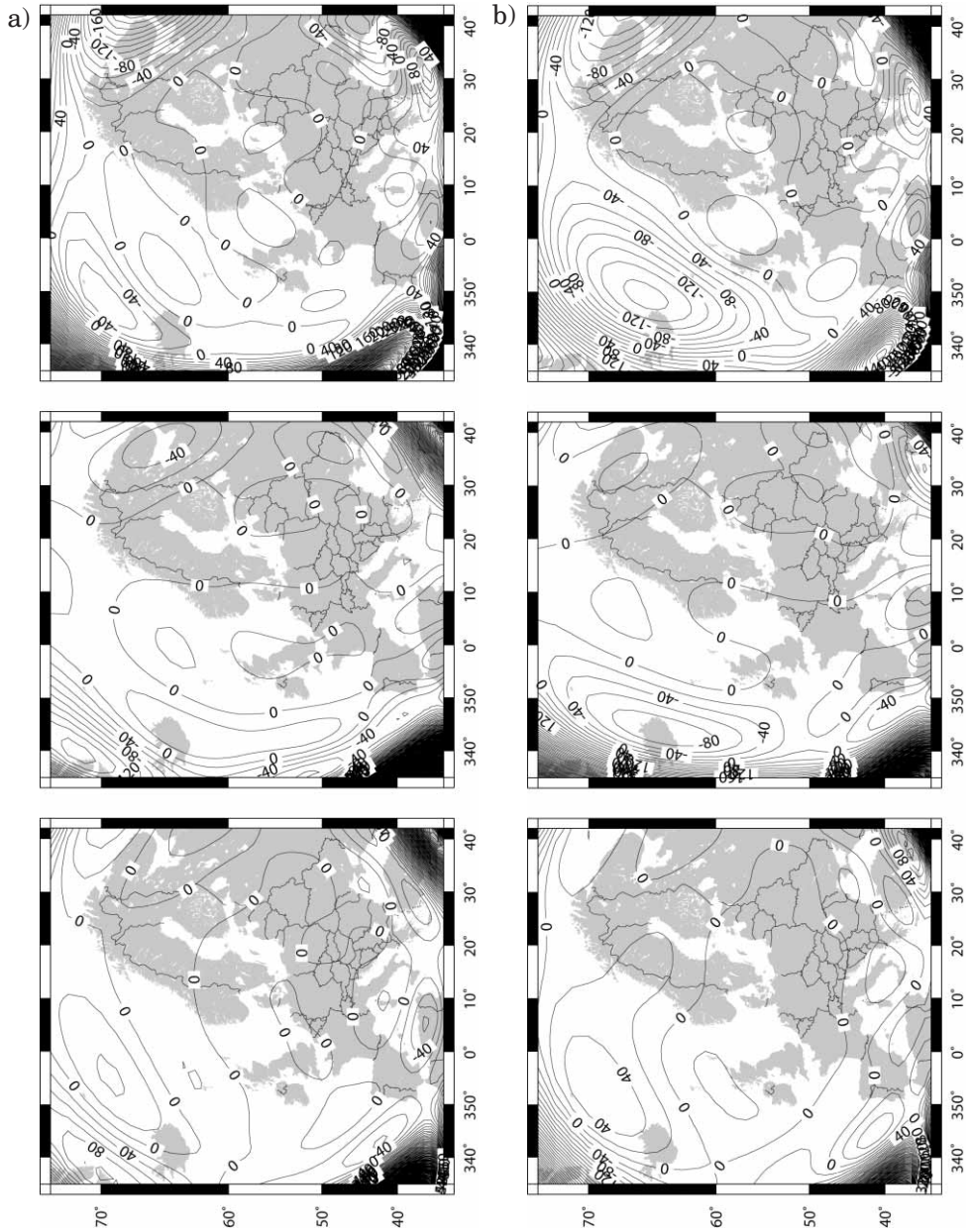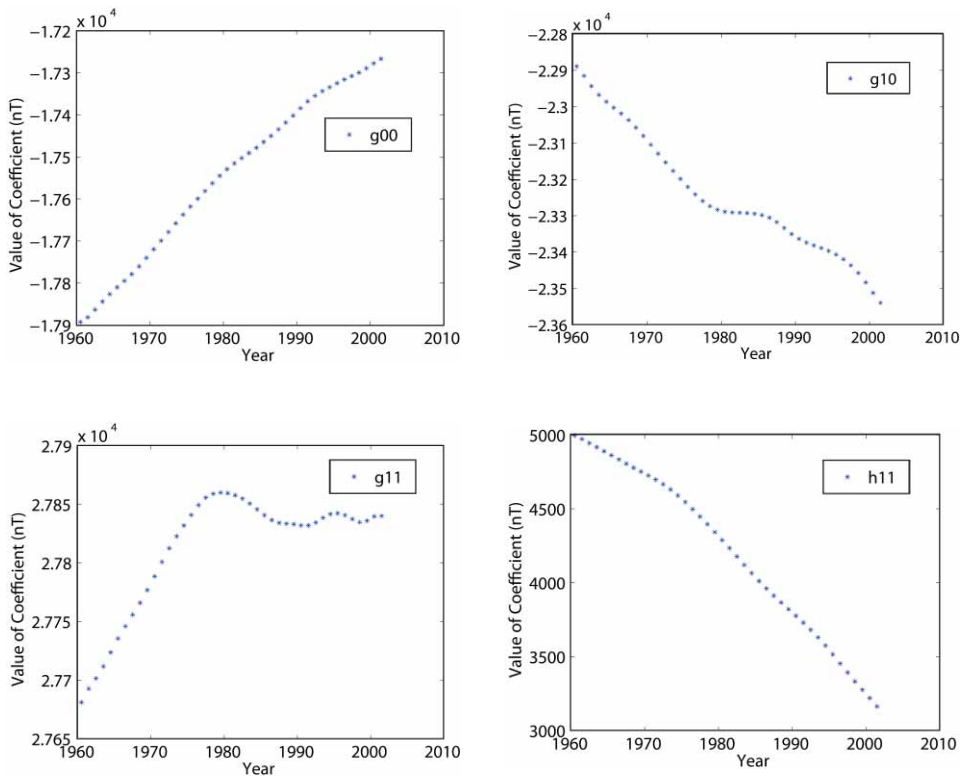
Figure 8. Maps for the *X* (left), *Y* (centre) and *Z* (right) residuals between EU_1X1_CM4 values and (a) CM4_OBS_VIR_NOR model and (b) CM4_OBS_VIR_R model. Units nT. Mercator map projection.

Figure 9. Time evolution of the CM4_OBS_VIR_R model coefficients.

prediction would be expected. It is clear that the additional virtual observatories constrained the dataset well, what is also confirmed by the reconstructed time-series. In Figure 11 the time series at two virtual observatories, VIR5 and VIR11 are presented, as examples of outermost locations.

5. Discussions and Conclusions

Promising results were obtained in modelling the magnetic field on regional scale when the original SCHA method with appropriate physical regularization was used (Korte and Holme, 2003). However, the data used in this previous study were not good enough to allow a confident interpretation of the results.

Accurate computation of the associated Legendre functions of non-integer degree is rather tough task and needs particular care. However this is a prerequisite for obtaining reliable results by means of SCHA. It is worth to note that the mentioned difficulty is not an intrinsic problem of SCHA, indeed the
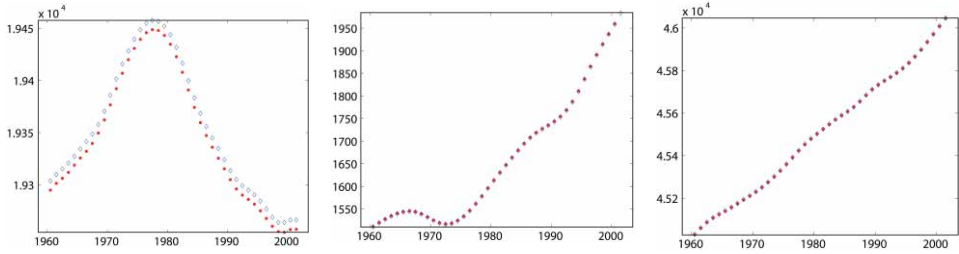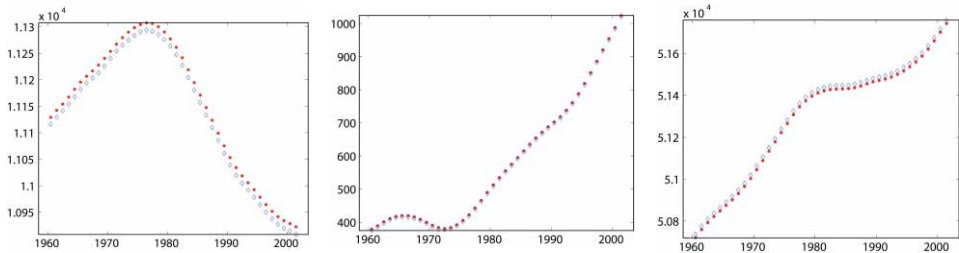
a)
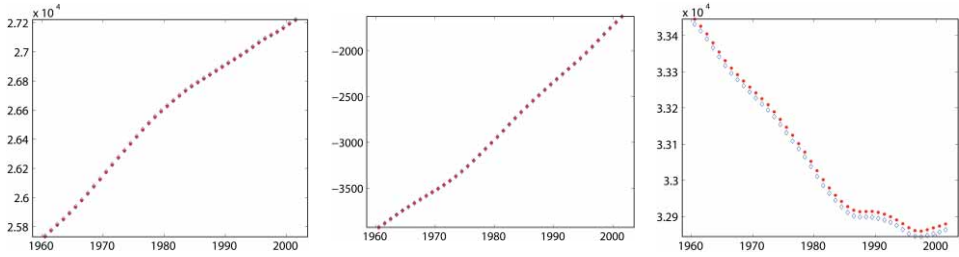
b)
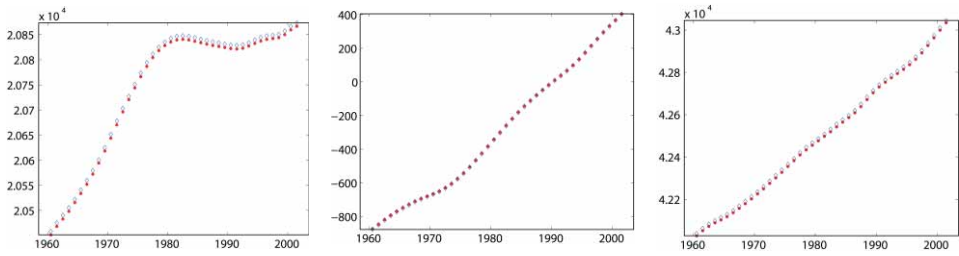
c)

d)

Figure 10. Time-series for X (left), Y (centre) and Z (right) components obtained from CM4_OBS_VIR_R model (full circles) and CM4 model (diamonds), in nT, at: (a) OBS1, (b) OBS2 (c) OBS2, (d) OBS3 and (e) OBS4 locations (see Fig. 1 for the locations).
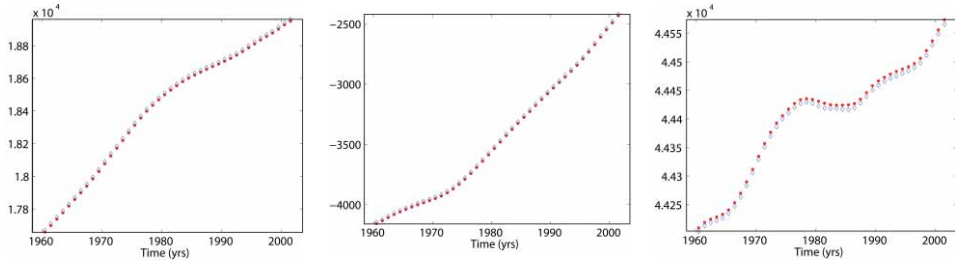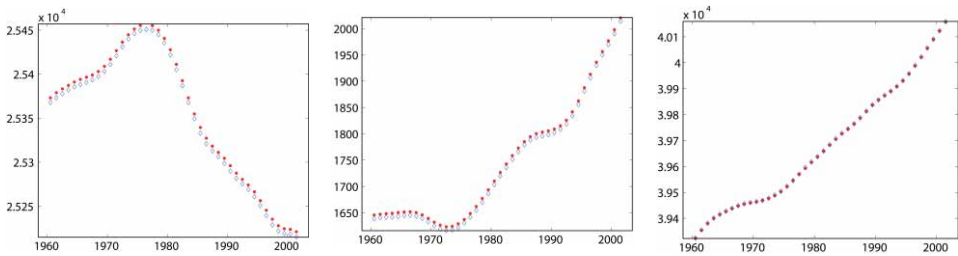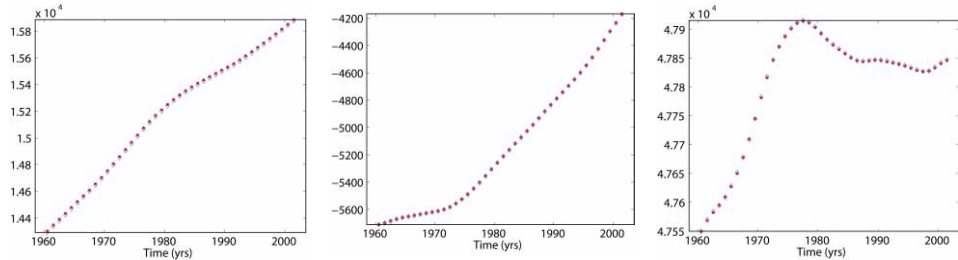
e)

Figure 10. continued.

a)

b)

Figure 11. Time-series for *X* (left), *Y* (centre) and *Z* (right) components obtained from CM4_OBS_VIR_R model (full circles) and CM4 model (diamonds), in nT, at: (a) VIR5 and (b) VIR11 locations (see Fig. 1 for the locations).

mathematical problem to accurate calculate the series with an infinite number of terms. The algorithm developed by Olwer and Smith (1983) offers a more stable way of computing these functions, especially for high values of the co-latitudes and degrees. Accurate computation of the associated Legendre functions together with the physical regularization which allows better smoothness and misfit of models, as well as simultaneously spatio-temporal modeling

with cubic splines are already a great improvement of the originally proposed SCHA method.

Here, I showed that it is possible to model the main field over a restricted region, as Europe is, with SCHA when appropriate model parameters are selected. I carefully investigated the following parameters: spherical cap harmonic angle, maximal degree of the spherical cap harmonic expansion, temporal splines, norms and regularization factors. The spherical cap half angle of 35°, centred at 53°N latitude and 14°E longitude defines well the area to be studied. Moreover, the margins are large enough around the cap preventing the influence of its boundary. The maximum degree of the spherical harmonic expansion was set to k_{max}= 8, this being the largest value allowed by data number and distribution. The size of the chosen cap along with k_{max} = 8 accounts for a good convergence of SCHA. Further, I showed that the artificial features resulting from the deficiencies of the method (mostly from the data distribution) are overcome when additional sites, 'virtual observatories', were carefully placed between the observatories and the cap boundary. Physical criteria for the amount of the smoothness of the magnetic field required by data were considered by choosing the combination of two norms, $\mathbf{B}^2$ and $(d\mathbf{B}/dr)^2$ (Korte and Holme, 2003), and appropriate spatial and temporal damping factors. Use of 20 splines was adequate for modelling a dataset covering 42 years (1960.5–2001.5).

Since the observatory time series contain unreported errors (Verbanac et al., 2006), I based this study on synthetic data, which can be considered as error-free. The uninterrupted time series over 42 years ensured good distribution in time domain, contributing to the higher reliability of the obtained model.

Four models were computed, two of them using synthetic dataset at 46 European observatory locations and two based on the same dataset complemented with data at 11 additional virtual sites. Using both datasets, models without and with regularization of the magnetic field, in space and time, were obtained. Even models without spatial regularization, CM4_OBS_NOR and CM4_OBS_VIR_NOR, were able to quite well reproduce the initial datasets. However, better results were obtained when some spatial smoothing was applied since the data distribution was not uniform (CM4_OBS_R and CM4_OBS_VIR_R models). When the additional, virtual observatories were added, a smaller spatial damping was required. The most prominent improvement was found in the Z component residuals, which were reduced to 20 nT in the area of interest. The rms of models with regularization decreased significantly when additional virtual observatory sites were considered, confirming that the encountered problems at the edges were due to the data distribution and not caused by the applied method (numerical instability). Moreover, it shows that regularization allows for a better fitting even with a larger dataset (see Table 1). Further, both regularization and additional virtual observatories reduced the total rms. In all investigated cases, owing to the uniform temporal

data distribution, the appearance of the models and misfits was little sensitive on the temporal damping. Among computed models, CM4_OBS_VIR_R model has the smallest total rms, showing again that with adequate data distribution and regularization the initial dataset is better described. In the area well covered with observatories, the residuals between original and modeled data (EU_1X1_CM4 and CM4_OBS_VIR_R) are not larger than 20 nT. All these arguments made us confident to chose the CM4_OBS_VIR_R model, as the preferred model.

The smooth temporal change of the first few SCHA coefficients and comparison of the time-series for X, Y and Z components of the original and modeled data at individual locations further confirmed its validity. Moreover, models computed for different epochs satisfy the proposed validation criteria. The rms values are similar to those shown in Table 1, confirming that the models are stable over the whole considered time span. This is also true for the epochs close to the beginning and the end of the analysed time interval. The computed values at the beginning and the end of the time interval, for both models, are less reliable as some edge effects could appear.

I plan to use the improved SCHA method explored in this study together with the carefully checked and improved main field dataset presented in Verbanac et al. (2007) to obtain a detailed secular variation model over Europe. The main field models obtained by SCHA, as presented here, will enable me to model the real magnetic data and then to derive secular variation models as the differences between successive main field values.

References

Alldredge, L. (1981): Rectangular harmonic analysis applied to the geomagnetic field. *J. Geophys. Res.* **86**, 3021–3026.

Chambodut, A., Panet, I., Mandea, M., Diament, M., Holschneider, M. and Jamet, O. (2005): Wavelet frames an alternative to spherical harmonic representation of potential fields, *Geophys. J. Int.*, (submitted).

Clark, T. (2000): *Introduction to Space Physics*. Cambridge University press.

de Boor, C. (1978): *A Practical Guide to Splines*. (ed.) Springer-Verlag, New York.

De Santis, A., Falcone, C. and Torta, J. M. (1997): SHA vs. SCHA for modelling secular variation in a small region such as Italy. *J. Geomagn. Geoelectr.,* **49**, 359–371.

Garcia, A., Torta, J. M., Curto, J. J. and Sanclement, E. (1991): Geomagnetic secular variation over spain 1970–1988 by means of sphericalcap harmonic analysis. *Phys. Earth Planet. In.*, **68**, 65–75.

Haines, G. V. (1985): Spherical cap harmonic analysis. *J. Geophys. Res.*, **90**, 2583–2591.

Haines, G. V. (1988): Computer programs for spherical cap harmonic analysis of potential and general fields. *Comput. Geosci.*, **14**, 413–447.

Haines, G. V. and Newitt, L. R. (1986): Canadian geomagnetic reference field 1985. *J. Geomagn. Geoelectr.*, **38**, 895–921.

Holschneider, M., Chambodut, A. and Mandea, M. (2003): From global to regional analysis of the magnetic field on the sphere using wavelet frames. *Phys. Earth Planet. In.*, **135**, 107–124.

Korte, M., Holme, R. (2003): Regularization of spherical cap harmonics. *Geophys. J. Int.*, **153**, 253–262.

Kotzé, P. B. (2001): Spherical cap modelling of Oersted magnetic field vectors over Southern Africa. Earth, *Planets and Space*, **53**, 357–361.

Macmillan, S., Maus, S., Bondar, T., Chambodut, A., Golovkov, V., Holme, R., Langlais, B., Lesur, V., Lowes, F., Lühr, H., Mai, W., Mandea, M., Olsen, N., Rother, M., Sabaka, T., Thomson, A. and Wardinski, I. (2003): The 9th-generation International Geomagnetic Reference Field. *Geophys. J. Int.*, **155**, 1051–1056.

Olwer, F. W. J. and Smith, J. M. (1983): Associated Legendre functions on the cup. *J. Comput. Phys.*, **51**, 502–518.

Sabaka, T., Olsen., N. and Purucker, M. (2004): Extending comprehensive models of the Earth's magnetic field with Oersted and CHAMP data. *Geophys. J. Int.*, **159**, 521–547.

Thébault, E., Schott, J. and Mandea, M. (2006): Revised spherical cap harmonic analysis (r-scha): Validation and properties. *J. Geophys. Res.*, **111**, BO1102, doi: 10.1029/2005JB003836.

Thébault, E., Schott, J., Mandea, M. and Hoffbeck, J. (2004): A new proposal for spherical cap harmonic modelling. *Geophys. J. Int.,* **159**, 83–103.

Thébault, E., Schott, J. J. and Mandea, M. (2002): Geomagnetic field modeling on small spherical caps. General Assembly EGS02–A–04673, SE6.07–1WE2A–003, Nice, France, EGS XXVII.

Torta, J. M., García, A., Curto, J. J. and Santis, A. D. (1992): New representation of geomagnetic secular variation over restricted regions by means of spherical cap harmonic analysis: application to the case of Spain. *Phys. Earth Planet. In.*, **74**, 209–217.

Verbanac, G., Korte, M. and Mandea, M. (2007): On long-term trends of the European geomagnetic observatory biases. *Earth, Planets and Space*, (In Press.).

SAŽETAK

O regionalnom modeliranju geomagnetskog glavnog polja

Giuli Verbanac

U ovom istraživanju primijenila sam Sfernu harmoničku analizu na kuglinoj kaloti, (*Spherical cap harmonic analyses*), SCHA, s fizikalnom regularizacijom na nizu sintetskih podataka koji su dobiveni CM4 modelom (*Comprehensive Model CM4*) (Sabaka i sur., 2004) na lokacijama 46 Europskih opservatorija i 11 dodatnih opservatorija koji su izabrani radi poboljšanja početne raspodjele podataka.

Glavni cilj bio je minimizirati poznate nedostatke SCHA metode i testirati razne efekte na rezultate modela, kako bi se pronašao pristup koji omogućuje bolji opis geomagnetskog glavnog polja i njegove sekularne promjene na regionalnom području. Također pokazujem da adekvatni izbor parametara modela (sferni kut kalote, maksimalni red harmonika, broj *spline* funkcija, norme i faktori prigušenja) zajedno s fizikalnom regularizacijom omogućuju da su izglađenost i odstupanje modela u skladu sa zahtjevima podataka. Odstupanje krajnog modela testirano je raznim kriterijima:

vrijednosti rms-a, vremenska evolucija koeficijenata, te usporedbom originalnih i modeliranih vremeskih nizova na svakoj lokaciji. Štoviše, modeli izračunati za razne epohe zadovoljavaju predložene kriterije validacije, potvrđujući nadalje stabilnost modela unutar čitavog razmatranog vremenskog razdoblja.

Ova studija otvara mogućnost detaljnog opisivanja regionalnog geomagnetskog polja i njegove sekularne promjene.

Ključne riječi: geomagnetsko polje, sekularna promjena, regionalno modeliranje, Sferna harmonička analiza, CM4 model

Author's adress: Giuli Verbanac, Department of Geophysics, Faculty of Science, University of Zagreb, 10000 Zagreb, Croatia, e-mail: verbanac@irb.hr